Acta Astronautica 107 (2015) 196–207

Contents lists available at ScienceDirect

Acta Astronautica

journal homepage: www.elsevier.com/locate/actaastro

Determination of temperature variation on lunar surface and subsurface for habitat analysis and design

Ramesh B. Malla*, Kevin M. Brown

Department of Civil and Environmental Engineering, University of Connecticut, 261 Glenbrook Road, Unit 2037, Storrs, CT 06269-3037, USA

ARTICLE INFO

Article history:
Received 19 June 2014
Received in revised form
13 September 2014
Accepted 28 October 2014
Available online 4 November 2014

Keywords:
Temperature and heat transfer
Lunar temperature profile
Lunar habitat
Lunar exploration
In-Situ Resource Utilization
Regolith

ABSTRACT

The ambient environmental factors present on the lunar surface pose some of the most difficult challenges for the success of a long-term human settlement on the Moon. Aside from the dangerous radiation levels and hypervelocity micrometeoroid impacts, the equatorial temperature on the surface of the Moon can range from 102.4 K to 387.1 K. These extremes pose a variety of complications like thermal expansion and contraction, which can, in turn, alter the static, dynamic, and frequency response of a structure. This paper first presents the analytical study of the surface and subsurface thermal/heat flow environments of a potential habitat site located at the Equator of the Moon using a general equation that was developed based on the thermodynamic principle of heat flow to determine the temperature variation/gradient with time as well as depth. This method was then applied, with appropriate modifications, to determine the temperature variation with time and through depth of a 1-m thick regolith shielding layer surrounding a lunar structure. The solution to the general equation was determined through the use of the fourth-order Runge–Kutta technique of numerical integration. The analysis results showed that the outermost layer of regolith fluff has very strong insulating capabilities causing the temperature to drop 132.3 K from the maximum daytime magnitude of 387.1 K within the first 30 cm at which point it then remains constant with increasing depth. At night, the temperature increases from the minimum magnitude of 102.4 K to 254.8 K within the outermost 30 cm. When considering a layer of regolith shielding atop a lunar habitat, the added albedo radiation input from the adjacent lunar surface to the structure increased the maximum daytime surface temperature to 457 K (about 70 K higher than the lunar surface temperature) and displayed a drop of 138 K within the first 30 cm depth of regolith cover. The minimum temperature at night increased 80.3 K over the surface temperature to reach 182.7 K while displaying an increase of 137.2 K through the outermost 30 cm. In general, throughout the lunar cycle, it was observed that at a fixed point in time, as the depth within the regolith increases, the temperature variation throughout the lunar cycle decreases and the temperature ultimately remains constant beyond a certain depth (observed to be approximately 30 cm). The framework of this study, which was completed considering a habitat at the lunar equator, can also be used at different locations of the Moon to study their adequacy for long-term colonization missions.

* Corresponding author. Tel.: +1 860 486 3683.
E-mail addresses: MallaR@engr.uconn.edu (R.B. Malla), kmb09020@engr.uconn.edu (K.M. Brown).

http://dx.doi.org/10.1016/j.actaastro.2014.10.038
0094-5765/

1. Introduction

The United States of America has identified six goals for pursuit under its national space programs. Among them are the energizing of competitive domestic industries for the advancement of space technologies, the expansion of international cooperation in space, and the improvement of stability within distant environments [1]. The continued pursuit of space technologies is the next step towards exploring the distant corners of the universe, be it by human or robotic initiatives.

The pursuit of these goals necessitates the advancement of lunar surface technologies leading to the eventual construction of a long-term human habitat on the surface of the Moon. The structural analysis and design of a base such as this brings on many challenges including protection from extreme temperature variations, hypervelocity micrometeoroid impacts, and dangerous levels of radiation exposure [2,3]. All of these potential threats are not commonly present to such extremes within the design of terrestrial structures. In addition to these environmental dangers, the habitat location, material selection, architectural layout, and safety mechanisms, among numerous other challenges must be clearly thought out and accounted for. Many of these design items have been investigated and explored previously by several different investigators [3–12].

On the lunar surface, there is an extended diurnal cycle lasting over 29 days resulting in long periods of extreme hot and cold temperatures. According to Vaniman et al. [2], it is estimated that during the daytime, temperatures can rise to 396.1 K (123 °C) at the equator while dropping as low as 40.1 K (−233 °C) within the shadowed polar craters during the night. Structures built in this environment can experience high amounts of expansion, contraction, and fatigue stresses, which must be accounted for within the design. Adequate shielding methods must also be incorporated to lessen the exposure and effects of the harsh lunar environment.

When compared to the Earth, studies suggest that the lunar interior is much less active in a variety of ways [13]. For example: (1) the topography at all scales is much older than the Earth, (2) there exist very few internal seismic sources combined with a relatively low coefficient of attenuation of seismic waves, (3) there exists no general lunar dipole magnetic field, and (4) the internal heat flux as measured from surface experiments is approximately half that of Earth. Early models of lunar temperature show that the central core temperature of the Moon has a temperature of approximately 1000 K [14].

Several lunar habitat concepts have been proposed by different research groups including, the Task Committee on Lunar Base Structures [3], Malla et al. [7–9], Ruess et al. [5], Benaroya et al. [4], Vanderbilt et al. [10], and Kennedy [11,12]. More recently, Malla and Chaudhuri [8,9], Malla and Gionet [15], and Malla and Brown [16,17] have proposed and analyzed two different frame-membrane structural system designs for long-term lunar habitation missions. A key component of these habitat systems is the use of In-Situ Resource Utilization (ISRU) through the use of lunar regolith as an environmental shield. A layer of lunar regolith 1 m thick surrounding the habitat is proposed, thereby protecting both the habitat itself and the crewmembers inside from the harsh environment. It is essential for the design of these structures to know how the temperature will vary through the depth of this regolith cover in order to accurately study the thermal stresses and deflections that can be expected within the frame.

This paper presents the study of the thermal environment at the Equator of the Moon and the temperature variation with time both on the lunar surface and at varying depths beneath the surface, using the thermodynamic principle of heat flow. Using the different input and output radiation sources present at the habitat site, including direct solar input radiation and both non-blackbody and albedo output radiation, a general thermodynamic equation is developed and furthermore solved using the fourth-order Runge–Kutta method of numerical integration. With this temperature profile known through a depth of regolith, it can be applied to the thermal shield surrounding the lunar habitat and its effect on the structural members can be investigated.

2. The NASA Apollo missions

During the NASA Apollo missions of the early 1970s, lunar subsurface heat flow experiments were completed in order to determine the temperature profile and the effective thermal conductivity of the lunar material [18]. It is on the basis of this series of experiments that the study presented in this paper is conducted. The Apollo missions used multiple experimental setups and equipment types whose results were replicated using mathematical theories and formulations. The experimentally determined temperature profiles from the Apollo missions are shown in Fig. 1.

At the Rima Hadley site (25.0° N, 3.0° E) used during the Apollo 15 expedition, the mean surface temperature measured was 207 K, which increased rapidly with depth to approximately 252 K at 90 cm [19]. During the lunar night, the temperature fell to 93 K. The topmost 2 cm was very loosely packed and experienced a high degree of temperature change with its depth. For this reason the regolith profile was divided into two gradations to provide a more accurate representation of the lunar surface material [19]. The uppermost had a thermal conductivity of 1.5×10^{-5} W/cm K and the compacted layer beneath had a conductivity of 1.4×10^{-4} W/cm K.

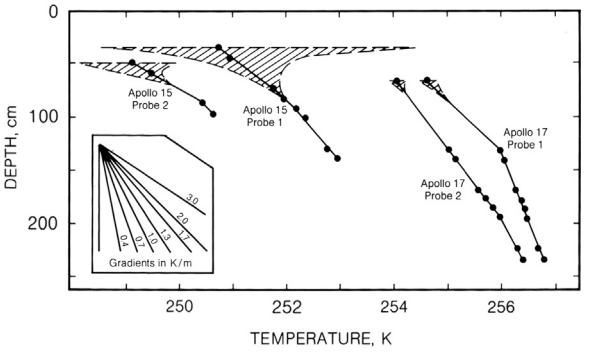

Fig. 1. Experimental lunar temperature profile [26].

At the Taurus-Littrow site (20.0° N, 31.0° E) used during the Apollo 17 mission, the mean surface temperature was 216 K [19]. Similar to Rima Hadley, the temperature increased rapidly to a temperature of 254 K at a depth of 67 cm. The minimum temperature experienced just before dawn was 103 K, slightly higher than that of Rima Hadley. Again the regolith profile was described to be of two layers of varying thermal conductivities, 1.5×10^{-5} W/cm K for the top 2 cm and greater than 1.2×10^{-4} W/cm K for the denser layer below. The density of the compacted regolith was approximately 1.8–2.0 g/cm^3 [19].

Following the Apollo missions, analytical studies were completed by Vasavada et al. [20] and Christie et al. [21] for the study of polar ice deposit stability on Mercury and the Moon and cryogenic fluid storage on the Moon respectively. Each study used a finite difference model for temperature determination with a system characterized by a 2 cm "fluff" layer atop a denser regolith layer that had different thermal properties as documented previously by Lauderdale and Eichelman [19] following a series of Apollo mission experiments. Their studies resulted in a temperature profile similar to each other and to the results of the Apollo experiments. Slight differences between them and this study can be attributed to the varying conditions used (location, phase, material properties, etc.).

3. Methodology for lunar surface and subsurface temperature determination

3.1. Lunar surface properties and heat sources

The lunar surface is comprised of two layers of lunar regolith of varying physical properties as determined during the Apollo 15 and 17 missions [19]. The top 2 cm consists of a loose regolith commonly known as "fluff." The fluff layer is characterized by a lower thermal conductivity ranging between 0.9×10^{-5} W/cm K at 0 K and 3.0×10^{-5} W/cm K at 400 K with an average density of 1.3 g/cm^3. Beneath this fluff layer lies regolith of a much higher compaction level and density equal to approximately 1.8–2.0 g/cm^3 and a thermal conductivity of 0.93×10^{-4} at 0 K to 1.94×10^{-4} W/cm K at 400 K. The thermal conductivity, k, varies with the temperature of the regolith as given by the following relationship [20]:

$$k = k_c\left[1+\chi\left(\frac{T}{350}\right)^2\right] \tag{1}$$

where T is the regolith temperature, χ represents the ratio of radiative to solid conductivity at temperature 350 K, and k_c is the solid conductivity. The values of k_c and χ were chosen in this study to agree with Vasavada et al. [20] and Cremers and Birkebak [22] who selected k_c values of 9.22×10^{-4} W/m K and 9.3×10^{-3} W/m K for the fluff and dense regolith respectively. The χ values used were 1.48 and 0.073 for the fluff and dense regolith layers respectively. The thermal conductivities stated previously within this section are in general agreement with those measured during the Apollo 15 and 17 missions to the Moon and by Vaniman et al. [2] (1.5×10^{-5} W/cm K for the upper 1–2 cm). The specific heat of each layer was taken to be temperature dependent using a constant bulk thermal inertia of 0.019 m^2 s$^{0.5}$ K/J which equals $(kpc)^{-1/2}$ where k is thermal conductivity, p is density, and c is specific heat [23,24].

Other studies have also been conducted that analyze lunar regolith and its thermal properties. Marov et al. [25] depict the thermal conductivity of lunar fluff as $k(T)=1.2\times10^{-3}$ W/m K$+T^3\times0.5\times10^{-10}$ W/m K^4. Fig. 2 displays the thermal conductivity of the lunar fluff and regolith layers as a function of temperature for both Eq. (1) and that given by Marov et al. [25] The conductivity of the fluff layer varies between the two formulas by 20–52% depending on the temperature, however, the resulting temperature profile of the regolith only varied by about 2% just below the 2 cm thick fluff layer. Due to this minimal change, Eq. (1) based on regolith samples from Apollo 12 was used for the study.

Fig. 3 depicts an illustrative representation of the thermal balance present at the lunar surface. The different input and output sources are described in further detail within Sections 3.2 and 3.3. In Fig. 3, the angle between the input direct solar radiation and a plane perpendicular to the lunar surface is defined as the angle of incidence, β_s.

3.2. Heat inputs

The Moon is exposed to a variety of different thermal input sources, which can greatly affect the temperature on

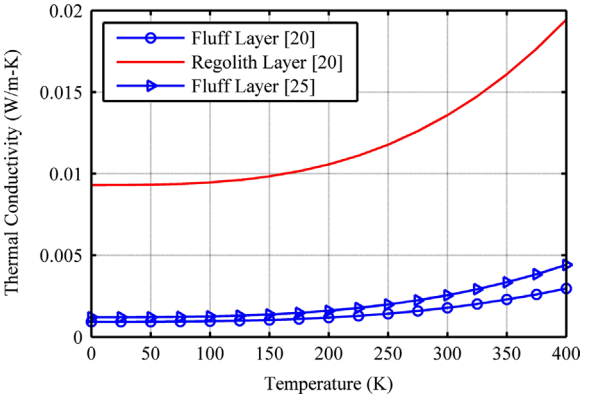

Fig. 2. Thermal conductivity of lunar regolith.

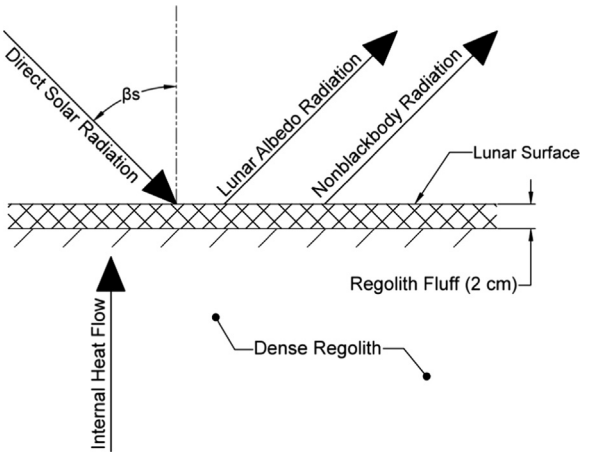

Fig. 3. Lunar surface thermal balance.

the surface. This thermal input consists of primarily direct solar radiation but also includes, to a lesser extent, an internal heat flow as well as a thermal input from the Earth (which has been neglected from this study due to its negligible magnitude when compared to the other input sources). Similar to the Earth, the temperature on the lunar surface varies greatly depending on the location, seen especially when comparing the equator to the poles. For this study, the habitat was constructed at the lunar equator, thus exposed to the maximum surface temperatures possible as well as a larger temperature variation [2]. The minimum temperature expected on the lunar surface exists within the deep polar craters, which receive minimal solar radiation. This case was not considered within this investigation because of its likely impractical nature for a preliminary habitation mission. Langseth and Keihm [26] also note that the temperature increases about 6 K from aphelion to perihelion due to the distance of the Moon from the Sun. Due to this relatively small value of the temperature change, this particular variable has not been considered in the analysis and the Sun–Moon distance is assumed constant throughout its revolution.

3.2.1. Direct solar radiation

The primary heat input source for the lunar surface is direct solar radiation. The solar heating power for the lunar regolith system is based on the material absorptivity of the lunar regolith as well as the solar radiation power of the Sun based on the Moon's location in orbit. The solar radiation power (G_s) per unit area incident at the lunar surface can vary from a maximum value of 1450 W/m^2 at lunar noon to the minimum value of 0 W/m^2 throughout the night [19]. Eq. (2) depicts the determination of the applied solar heating power as a function of the solar angle of incidence

$$G_s = G_{s,max} \cos(\beta_s) \tag{2}$$

where $G_{s,max}$ represents the maximum solar radiation power of 1450 W/m^2 and β_s is the solar angle of incidence. This variation in magnitude is based on the Moon's rotation and the associated angle of incidence (β_s) defined as the angle between the surface normal and the sun direction for the incoming radiation. The model developed for this study controls the solar radiation power magnitude (G_s) using a sine function as given by

$$G_s = \begin{cases} G_{s,max} \times \sin\left(\frac{2\pi}{t_c} t\right), & \text{Day} \\ 0, & \text{Night} \end{cases} \tag{3}$$

where t_c represents the time for a complete lunar phase cycle (approximately 29.53 days), and t represents the time during the lunar day. During the lunar night, the solar radiation power is set to zero ($G_s = 0$). The resulting solar energy flux is presented in Fig. 4 through two complete lunar cycles.

Upon reaching the surface, a portion of the direct solar radiation is absorbed while the remainder is reflected back into Space (albedo radiation). The amount of absorbed radiation is a function of the surface material absorptivity (a_s). For lunar regolith, the absorptivity was taken to be 0.87 [27]. Eq. (4) gives the applied solar heating energy, $\dot{q}_s$, that

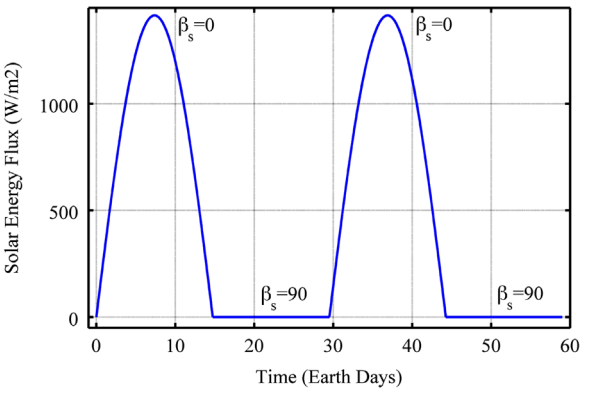

Fig. 4. Solar radiation power throughout lunar cycle.

reaches the lunar surface

$$\dot{q}_s = G_s A \tag{4}$$

where G_s is the solar radiation power given by Eq. (3), and A is the surface area receiving radiation. This value would then be multiplied by the surface absorptivity to determine the radiation entering the regolith system.

3.2.2. Internal heat flow

Similar to the Earth, materials within the lunar regolith create an internal heat flow due to the presence of various minerals within the soil [19]. Lunar samples taken during lunar surface missions have shown the presence of potassium and uranium isotopes, which are the primary sources of heat in both the Earth and the Moon [19]. Heat flow measurements and microwave emissions have shown the average internal heating power (G_i) to be equal to approximately 3.1×10^{-6} W/cm^2, which is, on average, about half that of the Earth (6.3×10^{-6} W/cm^2) [2]. The following relationship gives the total internal heating energy present:

$$\dot{q}_i = G_i A \tag{5}$$

where G_i is the internal heating power. Again, as done previously with the direct solar radiation within Section 3.2.1, this value would then be multiplied by the surface absorptivity to determine the radiation entering the regolith system.

3.3. Heat outputs

3.3.1. Nonblackbody radiation

All bodies within Space continually emit radiation energy in an amount related to its temperature and the overall nature of its surface. By definition, a blackbody surface is one which absorbs all of the incoming radiation and therefore has a surface absorptivity of $a_s = 1.0$. The Moon, because it does not absorb all of the radiation energy reaching its surface, is known as a nonblackbody surface defined by its surface absorptivity of $a_s < 1.0$. Nonblackbody surfaces are defined by their surface emissivity, which is defined as the ability of a surface to emit energy by radiation. The total emissive power of a nonblackbody surface, $\dot{q}_{nbb}$, can be

determined by the following relationship [28]:

$$\dot{q}_{nbb} = A\varepsilon\sigma T_s^4 \tag{6}$$

where σ is the Stefan–Boltzmann constant, T_s is the absolute surface temperature of the body, and ε represents the surface emissivity. The emissivity (ε) of lunar regolith has been measured to range from approximately 0.95 to 0.97 [20,21]. For this study a value of 0.97 was used.

3.3.2. Lunar albedo radiation

As stated within Section 3.2.1 with regard to incoming radiation, a portion of all solar radiation that impacts the lunar surface is reflected away back into Space. This radiation, known as albedo radiation, is characterized by the reflectivity of the lunar surface and the surfaces' designation as a nonblackbody surface. The total magnitude of lunar albedo radiation, $\dot{q}_r$, can be determined from the relation [29]

$$\dot{q}_r = \rho G_{s,max} A \cos(\beta_s) \tag{7}$$

where ρ represents the surface reflectivity.

Due to the opaqueness of the Moon, the transmissivity is equal to zero resulting in a surface reflectivity of 0.13 (the complement of the absorptivity taken as 0.87). For this reason, it is possible to define the surface reflectivity as $\rho = (1 - a_s)$.

3.4. Governing equation for temperature determination

In order to analytically determine the cycle of temperature variation to be expected on the lunar surface and below, a thermal analysis must be completed using the input and output heat sources described. The fundamental theories of conduction and radiation state that if a structure radiates heat outward, $\dot{q}_{out}$, and has a defined heat input, $\dot{q}_{in}$, then the thermodynamic differential equation of heat flow through the structure, in this case the lunar regolith system, is given by [30,31]

$$kV\frac{\partial^2 T(X,t)}{\partial X^2} - Mc\frac{\partial T(X,t)}{\partial t} = \dot{q}_{out}(X,t) - \dot{q}_{in}(X,t) \tag{8}$$

where k is the thermal conductivity of regolith, V represents the volume of regolith, t is the time, X is the depth in regolith, T represents the temperature at depth X at time t, M is the mass of regolith, and c signifies the specific heat of regolith.

Due to the relative uncertainty regarding many different properties of lunar regolith and the lunar surface, reasonable assumptions based on previous studies and measurements have been made for the magnitude of each of these parameters. Many of these selections have been included with their respective input/output formulas but are also summarized within Table 1.

Table 1
Lunar surface thermal parameters.

Parameter	Magnitude
Surface absorptivity, a_s	0.87
Solar radiation power, $G_{s,max}$ (W/m^2)	1450
Surface area, A (m^2)	2.25 (1 frame bay)
Solar angle of incidence, β_s	Varies from 0° to 90°
Internal heating power, G_i (W/m^2)	0.031
Surface emissivity, ε	0.97
Stefan–Boltzman constant, σ (W/m^2 K^4)	5.67e−8
Surface reflectivity, ρ	0.13
Regolith thermal conductivity, k	See Eq. (1)
Regolith specific heat, c	See Section 3.1

4. Surface temperature

For the purposes of this study, the lunar surface is defined as the outermost layer of lunar regolith, referred to as fluff. This layer is considered having uniform depth of 2 cm throughout the entire lunar surface. The location for the temperature profile determination on the Moon was taken to be at the Equator due to its maximum solar radiation input and resulting increased surface temperatures when compared to the lunar poles. Because this analysis is based on the lunar surface only and does not include depth, the general thermodynamic Eq. (8) can be simplified as follows:

$$-Mc\frac{\partial T(t)}{\partial t} = \dot{q}_{out}(X,t) - \dot{q}_{in}(X,t) = (\dot{q}_{nbb} + \dot{q}_r) - (\dot{q}_s + \dot{q}_i) \tag{9}$$

As shown and previously illustrated in Fig. 3, the input sources for the lunar surface include both direct solar radiation ($\dot{q}_s$) and internally generated radiation ($\dot{q}_i$). The output radiation sources are non-blackbody radiation ($\dot{q}_{nbb}$) and lunar albedo radiation ($\dot{q}_r$).

4.1. Steady-state temperature

Chapman [32] defines steady state as a particularly useful special case within thermodynamics in which there is no dependence of the system on time. With respect to the lunar surface, this definition leads to the simplification of Eq. (9) by setting the left side differential equal to zero. The resulting expression simply states that during steady state, the incoming heat sources, $\dot{q}_{in}(X,t)$, must be equal in magnitude to the outgoing heat sources, $\dot{q}_{out}(X,t)$. This results in no net gain or loss of heat within the system assuming ample time is provided for steady state to be reached. Eqs. (10a) and (10b) show the steady state relationship between the applicable heat sources for the lunar surface

$$\dot{q}_s + \dot{q}_i = \dot{q}_{nbb} + \dot{q}_r \tag{10a}$$

or

$$G_{s,max}A + a_s G_i A = A\varepsilon\sigma T_s^4 + (1 - a_s)G_{s,max}A \tag{10b}$$

By solving this relationship for the unknown variable T using the values shown in Table 1, the steady state temperature for the lunar surface was found to be 387.1 K (111.1 °C). This value will later serve as a boundary condition and initial data point for the numerical analysis performed to determine the temperature of the surface throughout the entire lunar cycle.

4.2. Solution technique: numerical analysis and integration

The method of approximation through numerical integration was used to solve the resulting differential equation shown in Eq. (11). This equation was obtained by directly substituting the appropriate input and output expressions into the general lunar surface equation shown in Eq. (9)

$$-Mc\frac{\partial T(t)}{\partial t}=\left(A\varepsilon\sigma T_s{}^4+(1-a_s)G_{s,max}\,A\cos(\beta_s)\right)-\left(G_{s,max}\,A\cos(\beta_s)+a_sG_iA\right) \tag{11}$$

Numerical integration based on the fourth-order Runge–Kutta procedure was used to solve this first order nonlinear differential equation. The Runge–Kutta method was adopted for the numerical technique due to its lower degree of error when compared to other methods of numerical integration [33]. A brief description is presented below to solve Eq. (11) using the Runge–Kutta method. Eq. (12a) shows a prototypical theoretical ordinary differential equation for the purposes of explanation, which can be modified as shown in Eqs. (12b) and (12c)

$$\frac{dy}{dt}=f(t,y),\quad y(t_0)=y_0 \tag{12a}$$

where

$$f(t,y)=\frac{1}{Mc}\left(\left(G_{s,max}\,A\cos(\beta_s)+a_sG_iA\right)-\left(A\varepsilon\sigma T_s^4+(1-a_s)G_{s,max}\,A\cos(\beta_s)\right)\right) \tag{12b}$$

$$y=T(t) \tag{12c}$$

where t_0 and y_0 are initial conditions of time and temperature respectively. Euler's method, which is the basis of the Runge–Kutta method, uses a truncated Taylor series to approximate the ordinary differential equation at hand. The Taylor series expansion of the unknown solution to Eq. (12) about the point $t=t_0$ is

$$y(t)=y(t_0)+(t-t_0)y'(t_0)+\frac{(t-t_0)^2}{2}y''(t_0)+\ldots \tag{13}$$

where $y'=dy/dt$, $y''=d^2y/dt^2$, etc. By retaining only the first derivative term and using the right side of Eq. (13), the numerical approximation of $y'(t_0)$ can be calculated and used to approximate $y(t_1)$. Once $y(t_1)$ is known, $y(t_2)$ can be approximated in a similar fashion, and so on. In general, the following recursive relation for $y(i)$ can be written [33]

$$y(i)=y_{i-1}+hf(t_{i-1},y_{i-1}),\quad i=1,\,2,\,\ldots,\,N \tag{14}$$

where $h=t_1-t_0$. In order to increase the accuracy of Euler's method, the magnitude of h must be reduced. This effectively causes the numerical solution to be evaluated more frequently thereby reducing the error in the solution. The fourth-order Runge–Kutta method uses the weighted average of four slope values to approximate the next point along the solution curve. The general formula for computing y_i from multiple slope estimates is [34]

$$y_i=y_{i-1}+\sum_{l=1}^{m}\gamma_l k_l \tag{15}$$

where γ_l are weighting coefficients and k_l are slopes evaluated at points in the jth interval. As stated, the fourth-order Runge–Kutta method uses four slope estimates calculated at each h-size step on the integration. These estimates, denoted as k_1, k_2, k_3, k_4 are calculated as [34]

$$k_1=f(t_{i-1},y_{i-1}) \tag{16a}$$

$$k_2=f\left(t_{i-1}+\frac{h}{2},y_{i-1}+\frac{h}{2}k_1\right) \tag{16b}$$

$$k_3=f\left(t_{i-1}+\frac{h}{2},y_{i-1}+\frac{h}{2}k_2\right) \tag{16c}$$

$$k_4=f(t_{i-1}+h,y_{i-1}+hk_3) \tag{16d}$$

from which a weighted average is calculated to determine the next value of y

$$y_i=y_{i-1}+h\left(\frac{k_1}{6}+\frac{k_2}{3}+\frac{k_3}{3}+\frac{k_4}{6}\right) \tag{17}$$

A computer program was created using MATLAB to automate this process at the given time step of 1 h throughout three complete lunar cycles (approximately 2100 computations).

4.3. Maximum surface temperature

Using the fourth-order Runge–Kutta analysis, the temperature profile shown within Fig. 5 was determined. The analysis began at lunar noon on the first day using the steady state temperature value of 387.1 K as the initial condition and ran until the completion of day three. For this investigation it was assumed that the lunar day and night are of equal length, 14.77 days.

During the daytime hours, the equatorial temperature reaches a maximum of 387.1 K at noon (point a), the midpoint of the lunar day. It is at this point where the input solar radiation is at a maximum as shown in Fig. 5. From this time onward, the temperature begins to decrease rapidly until the end of the lunar day where the temperature is approximately 185.6 K (point b). From here the rate of change in temperature begins to decrease, although very slowly at first, reaching a magnitude of 104.9 K midway through the night (point c). The remainder of the dark period sees little change in temperature reaching a minimum value of 102.4 K

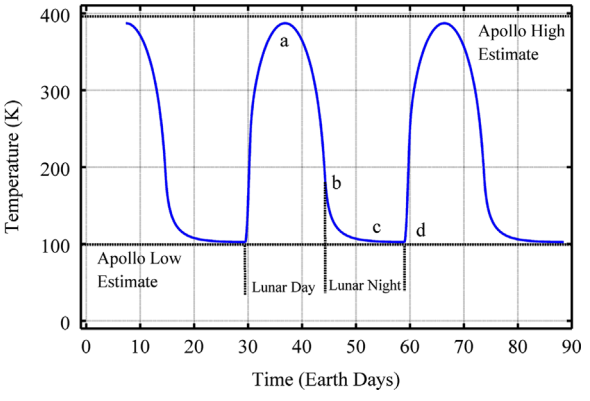

Fig. 5. Lunar surface temperature throughout lunar cycle.

Table 2
Lunar surface temperature comparison data.

Hours after Noon	Malla and Brown [17]	Christie et al. [21]	Vasavada et al [20]	Lauderdale and Eichelman [19]	
				Rima Hadley	Taurus-Littrow
0	387.1 K	386.0 K	392.0 K	396.0 K	396.0 K
6	185.6 K	145.0 K	148.0 K	N/A	N/A
12	104.9 K	95.0 K	108.0 K	N/A	N/A
18	102.4 K	85.0 K	100.0 K	93.0 K	103.0 K

(point d) before rising again very sharply to begin the daily cycle over again.

For further comparison, Table 2 shows the temperature data for four evenly spaced times throughout the lunar day as compared to the other previously published studies of Vasavada et al. [20] and Christie et al. [21], which were used for comparison throughout. The results of Apollo field experiments were also included [2,19]. As seen, there is a slight variation between the results of this study and those included for comparison; however, when dealing with a material such as lunar regolith this is not unexpected. Due largely to general unfamiliarity with lunar regolith and its material properties, a range of values is acceptable for use with many of the material properties including thermal conductivity, density, and specific heat. Different values for the maximum direct solar heat radiation power can also be found ranging from the 1414 W/m^2 used by Christie et al. [21] to 1450 W/m^2 noted by Lauderdale and Eichelman [19]. Due to this variation, the different studies used slightly different material properties, which may explain the slight difference in the temperatures shown.

5. Subsurface temperature

Of particular importance to the future design of a lunar habitat under thermal loading is the temperature at varying depths beneath the lunar surface. The methodology used for this purpose can be utilized to obtain the temperature profile through the depth of the regolith cover of the habitat. For a fixed point in time, the general thermodynamic equation, Eq. (8), considering only the change in depth (X) can be reduced to

$$kV\frac{\partial^2 T(X,t)}{\partial X^2} = \dot{q}_{out}(X,t) - \dot{q}_{in}(X,t) = (\dot{q}_{nbb} + \dot{q}_r) - (\dot{q}_s + \dot{q}_i) \tag{18}$$

To begin, this depth study was completed at a particular fixed time, noon, in order to study the effect of maximum temperature. However, the methodology is equally valid and can be applied for any other time. Next, the temperature was determined during the peak nighttime hour using the minimum surface temperature calculated during the lunar surface study in Section 4.3 as a boundary condition.

5.1. Solution technique: numerical analysis and integration

Similar to the surface temperature study of Section 4.3, fourth order Runge–Kutta techniques were used in the numerical integration of the thermodynamic equation, Eq. (18). Eq. (19) shows the complete equation solved for the daytime scenario including the input and output terms

$$kV\frac{\partial^2 T(X,t)}{\partial X^2} = \left(A\varepsilon\sigma {T_s}^4 + (1-a_s)G_{s,max}\,A\cos(\beta_s)\right) - \left(G_{s,max}\,A\cos(\beta_s) + a_s G_i A\right) \tag{19}$$

Because this equation is of the second order, before Runge–Kutta techniques can be used, Eq. (19) must first be transformed into a series of first order equations that can then be solved simultaneously as an initial value problem [32]. To do this, a new variable, Z, was introduced as follows

$$\frac{\partial T}{\partial X} = Z \tag{20a}$$

$$\frac{\partial Z}{\partial X} = \frac{1}{kV}\left[\left(A\varepsilon\sigma {T_s}^4 + (1-a_s)G_{s,max}\,A\cos(\beta_s)\right) - \left(G_{s,max}\,A\cos(\beta_s) + a_s G_i A\right)\right] \tag{20b}$$

To solve the system of equations, two initial conditions were used, the surface temperature, and the initial rate of change of the temperature with depth. This value was not known initially; however, by using the shooting method of numerical integration [34] and the previously discussed fourth-order Runge–Kutta method, the system of equations could be solved through the use of the known temperature well below the surface. Through the study of the Apollo mission's experimental results and those determined by Christie et al. [21] and Vasavada et al. [20], it was determined that the final temperature well below the surface would remain at a constant value, held there by the flow of radiation stemming from the Moon itself. The temperature used well beneath the surface was 254.8 K, midway between the peak daytime temperature of 387.1 K and the minimum nighttime temperature of 102.4 K.

In addition to this method, for further verification, the MATLAB function “bvp4c” was used to solve the thermodynamic equation as a boundary value problem [35]. The bvp4c function is a finite difference code that implements the three-stage Lobatto IIIa formula. This is a fully implicit Runge–Kutta method and a collocation formula. It results in a C^1 continuous solution of the fourth order.

5.2. Temperature variation with depth

5.2.1. Subsurface temperatures with extreme surface conditions

The results of the temperature profile through depth from the present study are shown in Fig. 6. Also shown are the results as calculated by Vasavada [20] and those collected on-site during the Apollo mission experiments. As shown in Fig. 6, the maximum temperature during the daytime analysis was 387.1 K determined from the previous lunar surface analysis along with the minimum temperature of 254.8 K.

Of primary importance here is the apparent effect of the 2 cm thick layer of fluff on the surface of the Moon. Largely due to the lower thermal conductivity, the fluff layer has a higher temperature shielding capability than

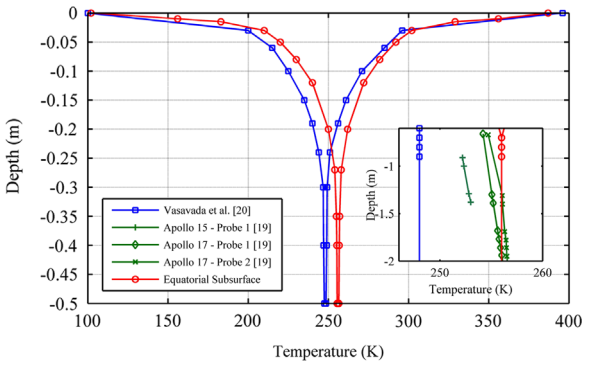

Fig. 6. Lunar subsurface temperature.

the underlying, compacted, regolith. Through the first 5 cm of depth (including the 2 cm fluff layer) the temperature dropped by nearly 25% to a magnitude of 292.1 K, a drop of 95 K. From this point on, the decrease in temperature was much more gradual resulting in the final constant temperature of 254.8 K after only 30 cm of total depth.

The resulting nighttime temperature profile was found to be quite similar to the daytime. Starting at 102.4 K, the temperature increased rapidly to a value of 209.4 K at a depth of 5 cm. A much more gradual increase in temperature led again to a constant value of 254.8 K at a depth of 30 cm.

From Fig. 6, it can be seen that the results obtained in this study are quite similar to both those of Vasavada [20] and of the Apollo missions. Vasavada [20] returned slightly higher and slightly lower surface temperatures during the daytime and nighttime respectively however this resulted in a constant temperature beneath the surface nearly identical to that calculated here. The overall trend of increasing and decreasing temperatures is also in general agreement. The Apollo data shown in the inset plot of Fig. 6 is also in high agreement with the present study. The temperatures are well within the acceptable range of difference, which can be expected due to the overall uncertainty and irregularity of the regolith material properties used. The primary difference seen is that the Apollo dataset shows a temperature, which continues to increase, albeit it very gradually, with depth well below the 30 cm limit analytically calculated.

5.2.2. *Subsurface temperature change with time*

The potential for fatigue stresses in the structural members necessitates the study of the temperature variation throughout the lunar diurnal cycle at particular depths of lunar regolith. This was done by repeating the original subsurface temperature analysis presented in Section 5.2, but only changing the initial condition of the surface temperature. The temperature at a depth well below the surface was maintained at the constant value of 254.8 K.

Fig. 7 depicts the results of this study at multiple depths including 0 cm (lunar surface), 5 cm, 15 cm, and finally 30 cm. As evidenced, even at the depth of 5 cm beneath the lunar surface, the temperature very closely resembles a sinusoidal curve. The extreme rise and fall during the daytime and the gradual decrease during the night are all but eliminated due largely to the presence of the fluff layer. In general, as the depth in regolith increases, the variation of temperature throughout the lunar cycle decreases resulting in a much steadier temperature profile.

5.2.3. *Surface temperature without regolith fluff*

While the Moon is covered with a thin layer of loosely compacted regolith fluff, it is possible that during the construction process of a lunar habitat, this layer will be removed thus altering the makeup of the regolith system. Fig. 8 shows the results of a subsurface analysis throughout the lunar cycle using only the properties of the densely compacted lunar regolith without a layer of fluff.

The results show further evidence of the strong insulating characteristics of the loosely compacted regolith fluff as shown in Table 3. When compared to the dense regolith only model, the temperatures at the various depths are significantly higher than those when including the fluff layer. Table 3 shows the comparison of the maximum and minimum temperatures found at different depths of the model. This difference is primarily due to the level of compaction of the regolith and the thermal conductivity of each material. With a lower density and thermal conductivity within the fluff layer, the flow of energy is reduced resulting in higher insulating abilities [28,32]. This finding shows that the high compaction and thermal conductivity of a dense regolith shield around a lunar habitat, in terms of thermal shielding, are actually less beneficial, which is a positive feature due to the inherent difficulties of regolith compaction within the lunar environment.

6. Habitat structural shielding system

Previously, two different frame-membrane habitat concepts have been developed and undergone a preliminary structural analysis for various different loading conditions. Fig. 9 shows a modular four-sided habitat whose dynamic

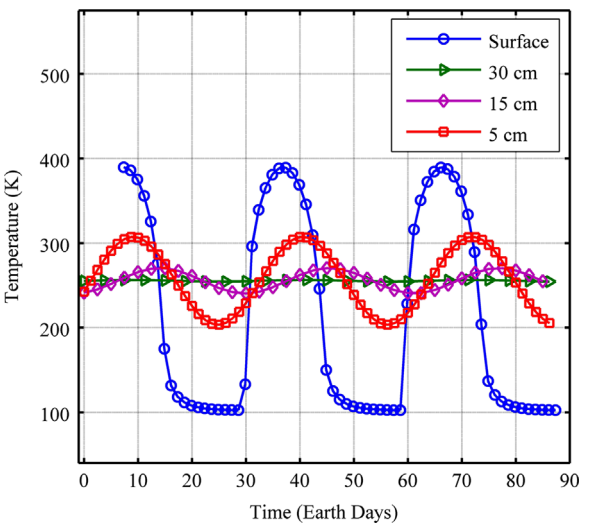

Fig. 7. Subsurface temperature variation throughout lunar cycle.

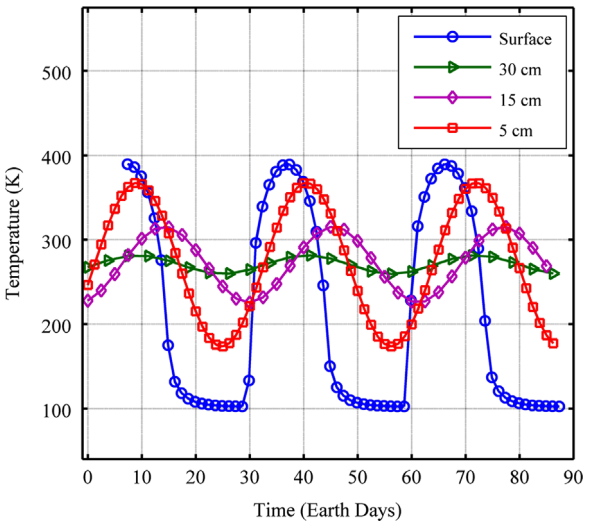

Fig. 8. Subsurface temperatures without regolith fluff.

Table 3
Effect of regolith fluff on subsurface temperatures.

Depth (cm)	Including fluff layer		Not including fluff layer	
	High	Low	High	Low
0 (surface)	387.1 K	102.4 K	387.1 K	102.4 K
5	304.1 K	203.4 K	365.0 K	180.5 K
15	275.4 K	234.1 K	315.2 K	214.3 K
30	254.8 K	254.8 K	280.7 K	258.8 K

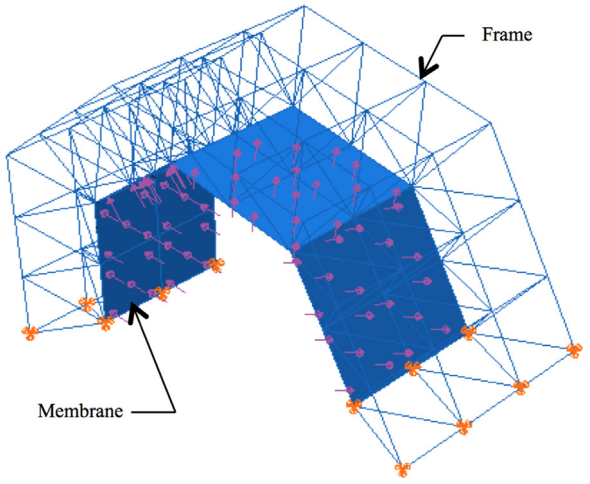

Fig. 9. Proposed habitat structure [8,9,15,36].

response to impact loading was studied [15]. Fig. 10 displays a rectangular habitat and airlock system, which is also used for this study. Previously the effects of self-weight, internal pressurization, and extreme temperatures were studied [16,17]. In order to create a habitable environment for use in a long-term lunar habitation mission, appropriate shielding must be installed surrounding the habitat. One method of shielding utilizing the in-situ resources is to provide a layer of lunar regolith around the structure.

With appropriate modification of the methodology presented for the lunar surface and subsurface temperature, the regolith shield surrounding the habitat interior was investigated. There exist two main differences to be considered for this version of the study: 1) the internal temperature of the habitat (293 K) will be considered as a boundary condition and 2) lunar albedo radiation from nearby surfaces will be considered as an additional input source subject to the same absorption coefficients as all other input sources. Fig. 11 shows this updated heat input/output model along with the aluminum frame of a proposed habitat.

6.1. Habitat surface steady state temperature

The habitat surface steady state temperature analysis is similar to that previously described for the lunar surface in Section 4.1. The difference is that the direct solar radiation reflected from the lunar surface (lunar albedo), $\dot{q}_r$, is now considered as an input for the habitat surface. As a result, the total output radiation reflected off of the habitat surface, $\dot{q}_{rs}$ given by Eq. (21b) below consists of two parts, one corresponding to the reflected portion of the direct solar radiation hitting the habitat surface and the other that corresponding to the solar albedo radiation coming from the nearby lunar surfaces. The steady state temperature can then be calculated by setting the input and output sources equal to each other as follows in Eq. (21b):

$$\dot{q}_{rs} = (1-a_s)\left[G_{s,\,max}\,A\cos(\beta_s) + (1-a_s)G_{s,\,max}\,A\cos(\beta_s)\right] \tag{21a}$$

$$\dot{q}_s + \dot{q}_i + \dot{q}_r = \dot{q}_{nbb} + \dot{q}_{rs} \tag{21b}$$

where the input radiation sources $\dot{q}_s$, $\dot{q}_i$, and $\dot{q}_r$ are defined by Eq. (4), Eq. (5), and Eq. (7), respectively; and the output sources $\dot{q}_{nbb}$ and $\dot{q}_{rs}$ are defined by Eq. (6) and Eq. (21a), respectively. This formulation results in a steady state temperature of 457 K for the lunar habitat.

6.2. Habitat shield surface temperature

Similar to the lunar surface temperature study in Section 4.2, the general thermodynamic equation, Eq. (8) was simplified to consider variation with time only. By substituting the appropriate expressions for the heat input to the habitat surface $\dot{q}_s$, $\dot{q}_i$, and $\dot{q}_r$, as given by Eq. (4), Eq. (5), and Eq. (6) respectively, along with the appropriate output heat expressions for $\dot{q}_{nbb}$ and $\dot{q}_{rs}$ defined by Eq. (6) and Eq. (21a), the habitat regolith shield surface temperature equation is obtained as below:

$$-Mc\frac{\partial T(t)}{\partial t} = (\dot{q}_{nbb} + \dot{q}_{rs}) - (\dot{q}_s + \dot{q}_i + \dot{q}_r) = A\varepsilon\sigma T_s^4 + (1-a_s)^2 G_{s,\,max}A\,\cos(\beta_s) - G_{s,\,max}A\,\cos(\beta_s) - a_s G_i A \tag{22}$$

Fourth-order Runge–Kutta numerical integration techniques were again used to numerically estimate the solution to this first order differential equation. The results of

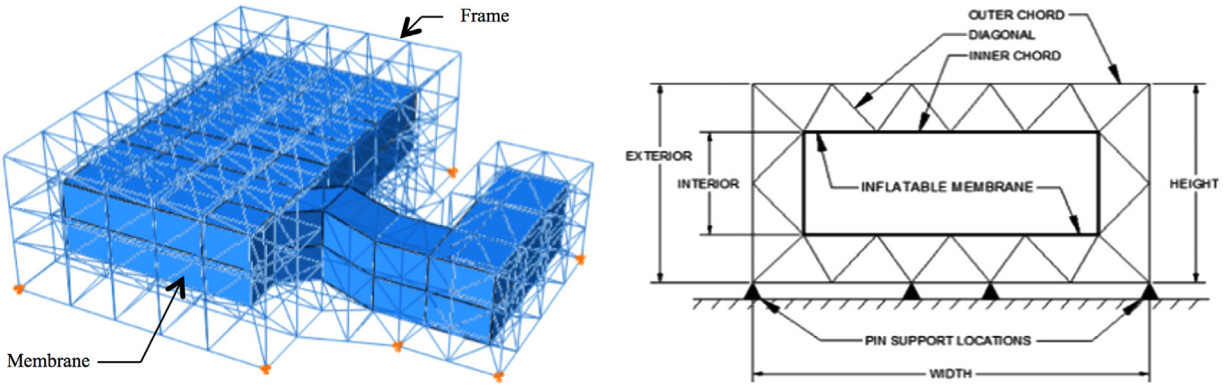

Fig. 10. Rectangular lunar habitat: (a) total structure, (b) main habitat cross-section [15,16].

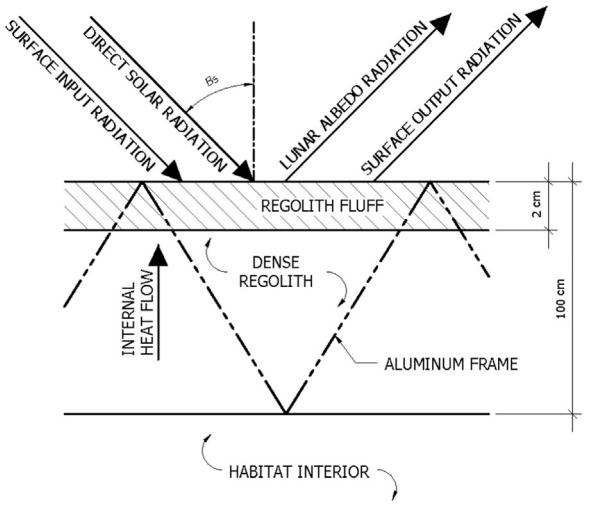

Fig. 11. Habitat regolith shield layer thermal balance.

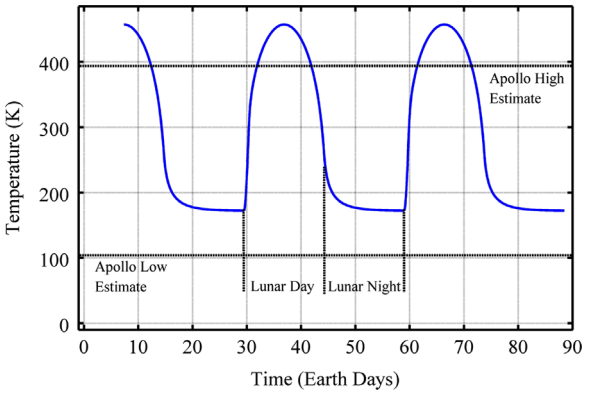

Fig. 12. Regolith shield surface temperature.

this are shown in Fig. 12. Beginning at the steady state temperature of 457 K at lunar noon, the temperature decreases significantly throughout the remainder of the daytime hours before leveling off and reducing at a much more gradual rate. The minimum temperature found during the nighttime hours was 182.7 K.

These temperatures are significantly higher than those calculated previously showing the overall power of the lunar albedo radiation. The maximum temperature is approximately 15% higher than the values measured on the surface by the Apollo crews.

6.3. Subshield temperature

6.3.1. Subshield temperatures considering extreme conditions

The solution method for this scenario is the same as the previous subsurface studies only with a different set in boundary conditions as mentioned previously and still using Eq. (18). This boundary value problem was solved using the calculated surface temperature and the known habitat interior temperature as the boundary conditions. The habitat interior is assumed to be at a constant room temperature of 293 K while the surface temperature will vary from 182.7 K at night to 457 K during the day. Fig. 12 shows the results of this instantaneous time study.

Fig. 13 shows that the temperature variation within the top 30 cm of regolith is identical to the surface study and unaffected by the interior boundary condition of 293 K. After reaching a nearly constant value 319.9 K approximately 30 cm deep, the temperature remains stable for about 45 cm. At this point the temperature decreases gradually for the remaining 25 cm until reaching its final magnitude of 293 K at the border of the habitat interior.

6.3.2. Temperature change with time through regolith shielding depth

For the eventual application of temperature loading to the structural members of the habitat frame, the temperature variation with respect to both depth and time was determined for the shielding scenario. Fig. 14 shows the results of this analysis considering the temperature at depths of 0 cm, 5 cm, 15 cm, and 30 cm.

Similar to the previous study, after only a small depth of 5 cm the general trends of the surface temperature are eliminated and the temperature profile is nearly sinusoidal. As the depth increases the amount of temperature variation at a particular depth decreases until it is eliminated at about 30 cm beneath the surface of the shield. Below this point, the regolith is unaffected by the input

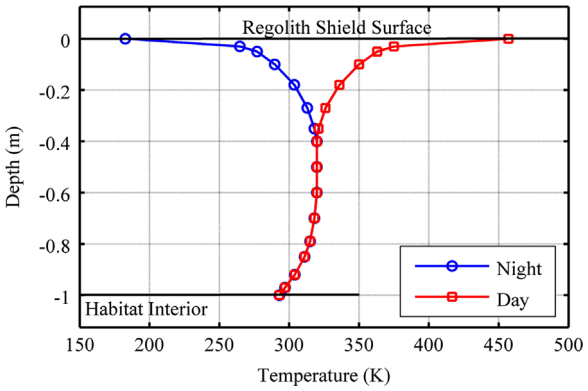

Fig. 13. Regolith habitat subshield temperatures.

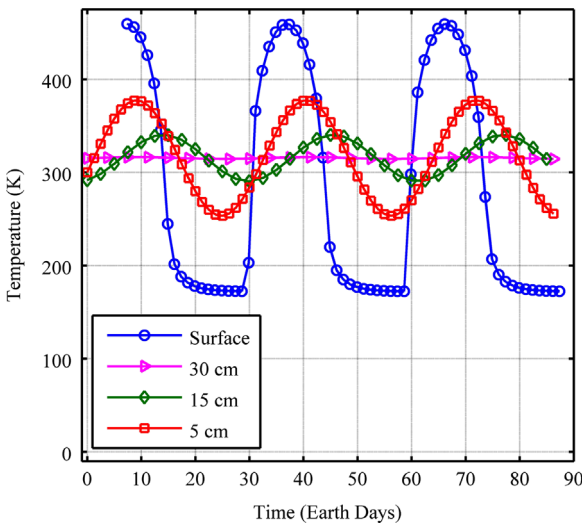

Fig. 14. Regolith habitat subshield temperature variation throughout lunar cycle.

radiation present at the surface and is only affected by the habitats interior temperature.

7. Summary and conclusions

During this investigation, the surface temperature of the Moon was analytically determined using the fourth-order Runge–Kutta numerical integration technique. With the surface temperature known, the temperature gradient through a depth of lunar regolith was determined for both day and night scenarios on the lunar surface and also on a 1 m thick regolith shield surrounding the lunar habitat, which may be present during a lunar habitation mission.

The surface of the Moon is subjected to both direct solar radiation as well as an internally generated heat flow originating in the presence of potassium and uranium isotopes with the regolith itself [2]. By equating the sum of these inputs with the system output generated by non-blackbody radiation, the steady state temperature was found to be 387.1 K at lunar noon. The results of the study showed a minimum equatorial surface temperature of 102.4 K just before the beginning of the daytime hours. The subsurface temperature profile results showed that only the outermost 30 cm of regolith was affected by the incoming radiation. The temperature decreased significantly through the 2 cm fluff layer before gradually decreasing to a constant value of 254.8 K at a depth of 30 cm. The trend showed that as the depth increased, the variation of temperature decreased.

Similarly, when considering a fixed depth of 1 m as a thermal shield atop a lunar habitat, the same general trends seen with the lunar surface model applied. The additional input of lunar albedo from adjacent surface conditions resulted in a surface temperature of 457 K with a minimum of 182.7 K. The effect of the surface radiation sources again only altered the temperature of the outermost 30 cm, while the innermost 25 cm of regolith was affected solely by the habitat's interior temperature being held at a constant 293 K.

Ultimately this study shows evidence that the thin layer of loose regolith fluff proves to be an important aspect to the In-Situ Resource Utilization (ISRU) shield. The temperature changed more rapidly within the 2 cm thick layer of fluff than it did within the denser layer beneath. This suggests that the compaction of lunar regolith for use as a shield might not only be difficult and potentially impractical in the lunar environment, but also undesirable altogether. A less dense and loosely compacted layer may prove more effective in terms of thermal shielding. The results of this study also correlate highly with previous studies completed as well as with data collected from various NASA run Apollo missions. By doing so, this study serves as an excellent representation of the lunar environment and therefore as a reliable source for the temperature data to be used in the structural design of a lunar habitat.

With this information known, it can be applied to a proposed lunar habitat concept for the purposes of structural analysis and design in preparation for a long-term colonization mission. Through this, an accurate representation of the applicable thermal expansion and contraction effects can be accommodated within the habitat design. It is anticipated that the thermal effects demonstrated here will affect both the required cross sectional dimensions of the frame members as well as the dynamic response of the structure. Both of these concepts have been demonstrated previously by Malla et al. [7–9,16,17,36]. A full frequency analysis is underway considering all of the applicable scenarios to fully understand the behavior of the structural system and adequately predict its behavior within the harsh environment of the Moon.

It should be noted that future studies in this subject matter should include more precise formulation of the problem at hand including the variation of additional parameters, which can affect the thermal conductivity and the flow of temperature through the lunar regolith. Some of these parameters include regolith density, porosity, and the bulk thermal inertia. A variable time boundary condition should also be considered when solving the unsteady heat conduction equation. By varying these properties, along with the temperature, in a more precise formulation, a very strong understanding on the flow of temperature through regolith can be gained.

Acknowledgments

The authors would like to gratefully acknowledge the financial support provided by the National Aeronautics and Space Administration (NASA) under its Ralph Steckler-Space Grant Space Colonization Research and Technology Development Opportunity Phase I, grant number NNX10AC21A, and the NASA Connecticut Space Grant Consortium in order to conduct this research. Additionally, the authors would like to acknowledge the University of Connecticut and its Department of Civil and Environmental Engineering located in Storrs, CT for their support throughout this research initiative.

References

[1] President of the United States, National Space Policy of the United States, ⟨www.whitehouse.gov/sites/default/files/national_space_policy_6-28-10.pdf⟩, ref. Nov. 16, 2013, Washington, D.C., 2010, pp. 1–14.
[2] D. Vaniman, R. Reedy, G. Heiken, G. Olhoeft, W. Mendell, The lunar environment, in: G. Heiken, D. Vaniman, B. French (Eds.), Lunar Sourcebook: A User's Guide to the Moon, Cambridge University Press, New York, 1991, pp. 27–60.
[3] Task Committee on Lunar Base Structures, Overview of existing lunar base structural concepts, J. Aerosp. Eng. ASCE 5 (1992) 159–174.
[4] H. Benaroya, L. Bernold, K.M. Chua, Engineering, design and construction of lunar bases, J. Aerosp. Eng. 15 (2002) 33–45.
[5] F. Reuss, J. Schaenzlin, H. Benaroya, Structural design of a lunar habitat, J. Aerosp. Eng. 19 (2006) 133–157.
[6] B. Sherwood, L. Toups, Technical issues for lunar base structures, J. Aerosp. Eng. 5 (1992) 175–186.
[7] R.B. Malla, H.R. Adib-Jahromi, M.L. Accorsi, Simplified design method for braced double-skinned structure in lunar application, J. Aerosp. Eng. 8 (1995) 189–195.
[8] R.B. Malla, D. Chaudhuri, Analysis of 3D frame-membrane structure for lunar base, in: R.B. Malla, W. Binienda, A. Maji (Eds.), Proceedings of the Earth and Space 2006: Engineering, Construction and Operation in Challenging Environments, ASCE, Reston, VA, 2006, pp. 1–8.
[9] R.B. Malla, D. Chaudhuri, Dynamic analysis of a 3-D frame-membrane lunar structure subjected to impact, in: W.K. Binienda (Ed.), Proceedings of the Engineering, Science, Construction and Operation in Challenging Environments, ASCE, Reston, VA, 2008, pp. 1–10.
[10] M.D. Vanderbilt, M.E. Criswell, W.Z. Sadeh, Structures for a lunar base, in: S.W. Johnson, J.P. Wetzel (Eds.), Proceedings of the Engineering, Construction and Operation in Space, ASCE, Reston, VA, 1988, pp. 352–361.
[11] K.J. Kennedy, Interior design of the lunar outpost, Proceedings of the Engineering, Construction and Operation in Space II, ASCE, Reston, VA, 1990, 529–540.
[12] K.J. Kennedy, A horizontal inflatable habitat for SEI, Proceedings of the Engineering, Construction and Operation in Space III, ASCE, Reston, VA, 1992, 135–146.
[13] J.A. Bastin, The lunar surface layer, Rep. Prog. Phys. 36 (1973) 289–346.
[14] D. Tozer, The moon's thermal state and an interpretation of the lunar electrical conductivity distribution, The Moon 5 (1972) 90–105.
[15] R.B. Malla, T. Gionet, Dynamic response of a pressurized frame-membrane lunar structure with regolith cover subjected to impact load, J. Aerosp. Eng. 26 (2013) 855–873.
[16] R.B. Malla, K. Brown, T. Filburn, Structural design of frame-membrane habitat concepts considering life support requirements for lunar colonization, in: Proc. 41st Int. Conf. Environ. Syst., AIAA, Reston, VA, 2011, pp. 1–13.
[17] R.B. Malla, K. Brown, Frequency analysis of a frame-membrane lunar habitat considering extreme temperatures and internal pressure, in: K. Zacny, R.B. Malla, W. Binienda (Eds.), Proceedings of the Earth and Space 2012: Engineering, Science, Construction and Operation in Challenging Environments, ASCE, Reston, VA, 2012, pp. 1400–1412.
[18] NASA News, Apollo 17 Press Kit, NASA, Washington, D.C., 1972.
[19] W.W. Lauderdale, W.F. Eichelman, Section 10: heat flow experiment, in: W.W. Lauderdale, W.F. Eichelman (Eds.), NASA TM X-58131 Apollo Scientific Experiments Data Handbook, NASA, Washington, D.C., 1974, pp. 10.6–10.49.
[20] A.R. Vasavada, D.A. Paige, S.E. Wood, Near surface temperatures on mercury and the moon and the stability of polar ice deposits, Icarus 141 (1999) 179–193.
[21] R.J. Christie, D.W. Plachta, M.M. Hasan, Transient Thermal Model and Analysis of the Lunar Surface and Regolith for Cryogenic Fluid Storage, in: NASA/TM-2008-215300, NASA, Cleveland, 2008, pp. 1–13.
[22] C.J. Cremers, R.C. Birkebak, Thermal conductivity of fines from Apollo 12, in: Proc. Lunar Planet. Sci. Conf., Lunar Planet. Inst., 1971, pp. 2311–2315.
[23] R. Smith, G. West, NASA TM-82478 Space Planetary Environment Guidelines for Use in Space Vehicle Development, NASA, Washington, D.C., 1983.
[24] G. Racca, Moon surface thermal characteristics for moon orbiting spacecraft thermal analysis, Planet. Space Sci. 43 (1983) 835–842.
[25] M.J. Marov, A.V. Kolesnichenko, V.N. Lebedev, K.K. Manuilov, On the Problem of Determining the Thermal Properties of the Soil of Phobos, Inst. Appl. Math., The Russian Academy of Science, Moscow, RU, 2007.
[26] M.G. Langseth, S.J. Keihm, In-situ measurements of lunar heat flow, in: Proc. Sov.—Am. Conf. Geochem. Moon Planets, NASA SP-370, NASA, Washington, D.C., 1977, pp. 283–293.
[27] E. Pettit, S. Nicholson, Lunar radiation and temperatures, Astrophys. J. 71 (1930) 102–135.
[28] L.C. Thomas, Heat Transfer, Prentice Hall, New Jersey, 1993.
[29] M.F. Modest, Radiative Heat Transfer, Academic Press, California, 2003.
[30] B.A. Boley, J.H. Weiner, Theory of Thermal Stresses, John Wiley and Sons, Inc., New York, 1960.
[31] H.S. Carslaw, J.C. Jaeger, General theory, Conduction of Heat in Solids, second ed. Oxford University Press, London, 1959, 1–49.
[32] A.J. Chapman, Heat Transfer, second ed. Macmillan Co., Inc., New York, 1974.
[33] G.W. Recktenwald, Numerical Methods With MATLAB Implementations and Applications, Prentice Hall, New Jersey, 2000.
[34] S.S. Rao, Applied Numerical Methods for Engineers and Scientists, Prentice Hall, New Jersey, 2002.
[35] The Mathworks Inc., MATLAB Mathematics R2013b, ⟨http://www.mathworks.com/help/releases/R2013b/ pdf_doc/matlab/math.pdf⟩, ref. Jan. 11, 2013, Natick, MA, 2013, pp. 11–28.
[36] R.B. Malla, T. Gionet, Frequency and impact analysis of a proposed frame-membrane lunar structure at extreme temperatures, in: Proc. 52nd Struct. Dyn. Mater. Conf., AIAA/ASME/ASCE/AHS/ASC, AIAA, Reston, VA, 2011, pp. 1–22.